Faceting of Twin Grain Boundaries in High-Purity Copper Subjected to High Pressure Torsion

Anna Kosinova, Boris Straumal,* Askar Kilmametov, Petr Straumal, Marat Bulatov, and Eugen Rabkin

The microstructure of high-purity 5N5 copper processed by high pressure torsion (HPT) is studied. Close to the top and bottom surfaces of HPT disk, the 2–10 µm-thick ultrafine-grained layers with equiaxial grains and grain size of about 150 nm are formed. This grain size is typical for HPT of copper and its alloys. However, the remaining bulk layer in the HPT disk contained mainly elongated intersecting twins with high aspect ratio and length of up to 1 µm. These twin grain boundaries (GBs) are faceted. The geometry of the GB facets is analyzed using Σ3 coincidence site lattice (CSL). The Σ3 twins after HPT contained $(100)_{CSL}$, $(110)_{CSL}$, $(010)_{CSL}$, and non-CSL $9R$ facets, but not $(120)_{CSL}$ and $(130)_{CSL}$ facets. Earlier, the stability diagram for the Σ3 GB facets is experimentally constructed for the same 5N5 high-purity copper. The comparison of the data with this diagram allows to estimate for the first time the effective temperature of pure copper during HPT processing at room temperature (RT): $T_{eff} = 920 \pm 50$ K. In other words, the HPT at RT results in Σ3 GB facets as if the sample is annealed at $T_{eff} = 920 \pm 50$ K.

1. Introduction

During severe plastic deformation (SPD), the geometric conditions do not allow the fracture of the material subjected to ultra-high strain. As a result, the amount of lattice defects in the material undergoing SPD continuously increases until a certain dynamic equilibrium between defects production and annihilation is established. Such steady state is characterized by the increased concentration of lattice defects (vacancies, interstitials, dislocations, grain, and interphase boundaries, etc.)[1,2] and constant value of torsion torque,[3–6] grain size,[7–25] Vickers microhardness,[7,11,26–38] and tensile strength.[28,31,39–41] In some experiments, the concentration of excess defects has been directly measured in situ during SPD (e.g., with the aid of synchrotron X-rays).[42,43] However, there are a number of indirect methods allowing one to observe the effects of increased defects' concentration during SPD. It is well known that some lattice defects (such as vacancies) can reach their equilibrium concentration at elevated temperatures, and that their concentration exponentially increases with increasing temperature.[44–46] SPD performed at T_{SPD} equal to room temperature (RT) can lead to the same state of material as if this material has been annealed at a certain elevated temperature (sometimes called effective temperature T_{eff}).[47] From this point of view, SPD is similar to severe irradiation with neutrons or ions,[48] or to severe deformation by high-energy ball milling.[49] For example, after SPD performed at T_{SPD} equal to RT, the deformed samples can contain phases which are in equilibrium at an elevated T_{eff}. These are, for example, a solid solution with high concentration of second component,[50] intermetallic compounds stable at $T > RT$[51,52] and amorphous

Dr. A. Kosinova, Prof. E. Rabkin
Department of Materials Science and Engineering
Technion-Israel Institute of Technology
Haifa 3200003, Israel

Prof. B. Straumal
Institute of Solid State Physics
Russian Academy of Sciences
Chernogolovka 142432, Russia
E-mail: straumal@issp.ac.ru

The ORCID identification number(s) for the author(s) of this article can be found under https://doi.org/10.1002/adem.201900589.

Prof. B. Straumal, Dr. A. Kilmametov
Department of Materials Science
Chernogolovka Scientific Center of Russian Academy of Sciences
Chernogolovka 142432, Russia

Prof. B. Straumal, Dr. A. Kilmametov
Karlsruhe Institute of Technology
Institute of Nanotechnology
Eggenstein-Leopoldshafen 76344, Germany

Prof. B. Straumal, Dr. P. Straumal
Department of Physical Chemistry
National University of Science and Technology «MISIS»
Moscow 119049, Russia

Dr. M. Bulatov
Department of Materials Science
Scientific and Technological Centre of Unique Instrumentation of the Russian Academy of Sciences
Moscow 117342, Russia

phase(s).[53,54] Another example is related to the accelerated mass transfer. One can estimate, for example, the number of atoms needed for the SPD-induced dissolution or precipitation of particles of a second phase. Knowing the duration and distance of such SPD-induced mass-transfer, one can estimate the value of equivalent diffusion coefficient (for the bulk D_b or grain boundary diffusion D_{GB}).[47,55–57] These estimated values are many orders of magnitude higher than D_b or D_{GB} extrapolated to T_{SPD} despite the fact that high pressure (in case of high pressure torsion [HPT]) strongly decreases the rate of mass transfer.[58,59] They are close to D_b or D_{GB} at a certain elevated T_{eff}. It is important to underline that the T_{eff} values calculated from the comparison of phases with an equilibrium phase diagram are very close to those calculated from the data on mass transfer.[47,55–57] An additional way to estimate T_{eff} is to use the phenomenon of grain boundary (GB) segregation of a second component.[60,61] However, the aforementioned three methods for the estimation of T_{eff} are applicable only for the (at least diluted) alloys.

In this work, we propose a new way to estimate T_{eff}, namely, with the aid of the so-called GB faceting–roughening transition.[62] Indeed, it has been shown that the equilibrium shape of $\Sigma 3$ and $\Sigma 9$ GBs depends on the temperature.[63] With decreasing temperature, the number of crystallographically different facets in $\Sigma 3$ and $\Sigma 9$ GBs increases.[64] Moreover, the GB premelting and prewetting transitions[65–67] can in turn influence the GB energy and faceting.[68] We observed recently that during HPT of a very high-purity 5N5 copper, the dynamic recrystallization takes place in the interior areas of an HPT disk.[69,70] As a result, it contains quite long twins where the facets are visible and shape of $\Sigma 3$ GBs can be analyzed.[70] In this work, we will analyze the facets in $\Sigma 3$ GBs in 5N5 copper after HPT, compare them with equilibrium phase diagram for the $\Sigma 3$ GB faceting–roughening constructed in the study by Straumal et al.[64] for the same material and, in such a way, estimate T_{eff} for the pure metal.

2. Results

The GBs with misorientation angles $\theta > 15°$ are usually considered as high-angle GBs. The low-angle GBs with $\theta < 15°$ can be described as an array or arrays of lattice dislocations. However, for $\theta > 15°$ the cores of lattice dislocations overlap. Thus, for $\theta > 15°$, a GB cannot be represented as an array of 1D lattice defects anymore and has to be treated as a true 2D lattice defect. Moreover, for certain misorientations θ_Σ called coincidence misorientations, a part of the lattice sites of the grain 1 coincides with the lattice sites of its misoriented counterpart, the grain 2. Thus, a pair of θ_Σ and misorientation axis defines so-called coincidence site lattices (CSLs).[71] The CSL is a superlattice for grains 1 and 2. A CSL can be described by a parameter Σ, which is the inverse density of coincidence sites. For example, for $\Sigma 3$ misorientation each third lattice site of a grain 1 coincides with a lattice site of a grain 2. The GBs for low-Σ misoreintations that contain a high number of coincident sites per unit of length exhibit the periodic structure and are called coincidence GBs. The coincidence GBs usually exhibit low energy, migration rate, diffusion permeability, and high strength.[72,73] Coincidence GBs are usually faceted. In other words, a curved GB breaks into a sequence

of flat segments. The free surfaces of the crystals can also facet. Such surface facets are usually observed in crystals with high Peierls barrier, they are parallel to the low-index, densely packed lattice planes.[72,74–76] The GB facets usually correspond to the CSL planes with highest density of coincident sites.

One can observe the transition between faceted and rough surfaces (or GB). Such faceting–roughening phase transformation can occur, for example, during the temperature increase. The GB faceting–roughening phase transformation is similar to that of free surfaces.[77–79] The temperature increase leads to the decrease in Gibbs free energy of an individual step on a flat surface facet. At a certain temperature T_R, the step energy vanishes. If a step energy is zero, such flat facet cannot be stable because of the spontaneous formation of steps. Thus, if T_R of a certain surface is below the melting temperature T_m, then above T_R such surface becomes rough. This is the faceting–roughening transition.[80,81] Such GB roughening transition of the first order has been observed in $SrTiO_3$ between 1773 and 1873 K.[79] The roughening transition of the second order in $\Sigma 3$ GBs in molybdenum has been reported.[82] Theory predicts that T_R is high for the facets with high step energy and vice versa.[80,81] Indeed, the facets that are densely packed with lattice sites have high step energy and high T_R. A sequence of three roughening transitions with different T_R for free surfaces has been observed only in solid helium.[83] For GB facets, a CSL plays a role similar to that of crystal lattice for the surface facets. Indeed, it was observed that the new GB facets with decreasing density of coincidence sites appear with decreasing temperature.[64] Above $0.75 T_m$, the $\Sigma 3$ GBs in pure copper contain only two crystallographically different facets.[64]

In **Figure 1**, the sections of the CSL patterns perpendicular to the common [110] tilt axis for two misoriented grains 1 and 2 are shown. The micrographs of respective intersections of $(100)_{CSL}$ GB facet with other facets are also shown. The micrographs were obtained on the specially grown stress-free bicrystal with tubular $\Sigma 3$ GB.[64] The lattice sites or the grains 1 and 2 are shown with open and solid symbols, respectively. The coincidence sites and nodes of $\Sigma 3$ CSL are shown by large circles. In all schemes in Figure 1, the $\{111\}_1/\{111\}_2$ or $(100)_{CSL}$ CSL plane that is most closely packed with CSL nodes is shown. In Figure 1b–e, the CSL planes that are less densely packed with CSL nodes are shown as well. These are $(010)_{CSL}$ facet (Figure 1b), $(110)_{CSL}$ facet (Figure 1c), $(120)_{CSL}$ facet (Figure 1d), and $(130)_{CSL}$ facet (Figure 1e). The $\Sigma 3$ twin GBs can also possess the non-CSL, so-called $9R$ facets (Figure 1a). These $9R$ facets at the end of twin lamellae form an angle of 82° with $(100)_{CSL}$ plane. Such 82° facets are not parallel to any low-index $\Sigma 3$ CSL plane. The energy minimum at 82° is due to the formation of thin GB layer with so-called $9R$ structure forming a layer of body-centered cubic (BCC) GB phase in the FCC matrix.[84–87]

After HPT of high-purity 5N5 copper, the layers of ultrafine grains are formed close to both surfaces of HPT disk.[69,70] The grain size in this surface layers was close to the grain size after HPT in copper of lower purity and copper-based alloys, namely 150–250 nm.[88–94] Deep in the HPT disk, the dynamic recrystallization took place during HPT, and the larger grains are formed (see scanning electron microscopy [SEM] micrograph in **Figure 2**a). We compared the grain size distribution in the samples immediately (1–3 h) after HPT and after keeping the
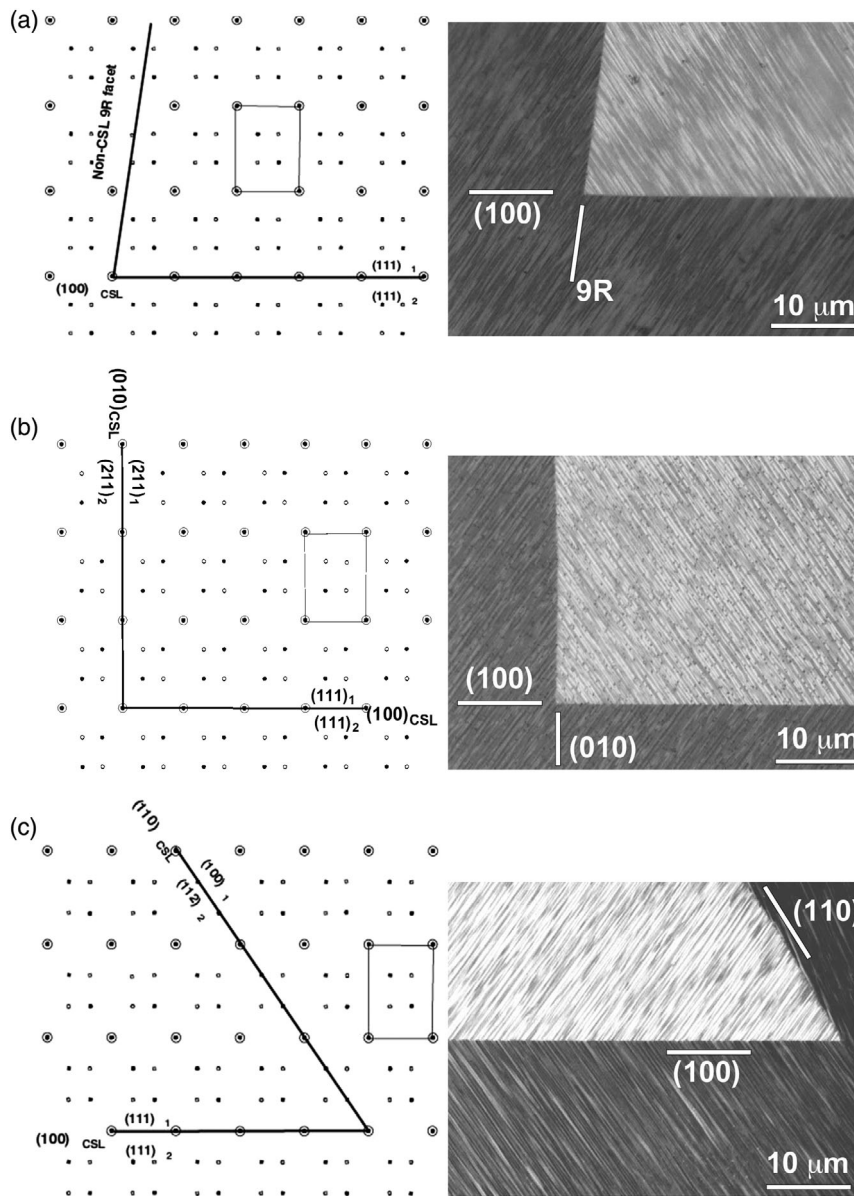
1900589 (2 of 8)

**ADVANCED
SCIENCE NEWS**

www.advancedsciencenews.com

**ADVANCED
ENGINEERING
MATERIALS**

www.aem-journal.com

Figure 1. Sections of Σ3 CSL perpendicular to the {110} tilt axis with position of various facets (left) and micrographs of intersections of $(100)_{CSL}$ with other facets (right).[64] a) $(100)_{CSL}$ and 9R facets; b) $(100)_{CSL}$ and $(010)_{CSL}$ facets; c) $(100)_{CSL}$ and $(110)_{CSL}$ facets; d) $(100)_{CSL}$ and $(120)_{CSL}$ facets; and e) $(100)_{CSL}$ and $(130)_{CSL}$ facets. Reproduced with permission.[64] Copyright 2006, Elsevier.

samples about 6 months at RT. We did not observe any measurable changes in the grain size distribution. It means that the large grains indeed resulted from the dynamic recrystallization and grain growth during HPT. Such dynamic recrystallization during SPD have also been observed earlier in other materials like titanium-based,[95–97] magnesium-based,[98–102] aluminum alloys,[103–106] copper alloys,[106] and nickel-based superalloys.[107] These large recrystallized grains are predominantly typical twins intersecting with each other. The side facets of the long twin plates are the $\{111\}_1/\{111\}_2$ or $(100)_{CSL}$ CSL planes. The $(100)_{CSL}$ CSL planes have highest density of CSL nodes. The $(100)_{CSL}$ facets are marked by arrows in higher-magnification micrographs in Figure 2b–d. Together with $(100)_{CSL}$ facets, the twin GBs

contain also the short facets with other orientations (or inclinations). Such short facets are also marked by arrows in Figure 2b–d. We identified them basing on the schemes given in Figure 1. Thus, the 9R $(010)_{CSL}$ and $(110)_{CSL}$ facets are visible in the micrographs in Figure 2b–d together with $(100)_{CSL}$ facets. The $(120)_{CSL}$ and $(130)_{CSL}$ facets observed in pure copper in the study by Straumal et al.[64] are not present in our samples.

3. Discussion

It has been recently demonstrated that SPD can drive various phase transformations in materials.[50–54] In particular, these
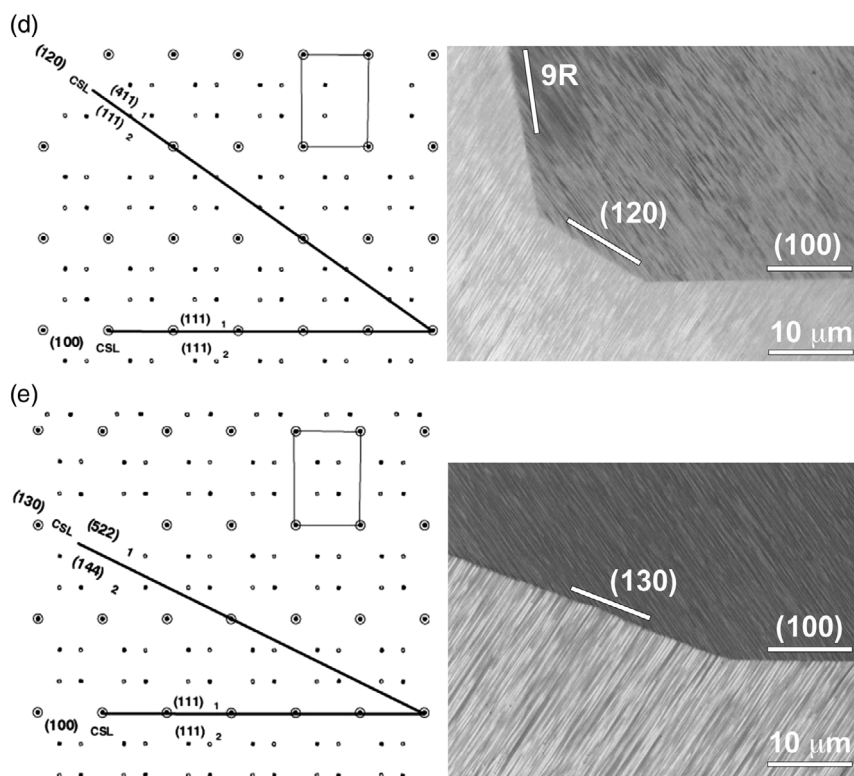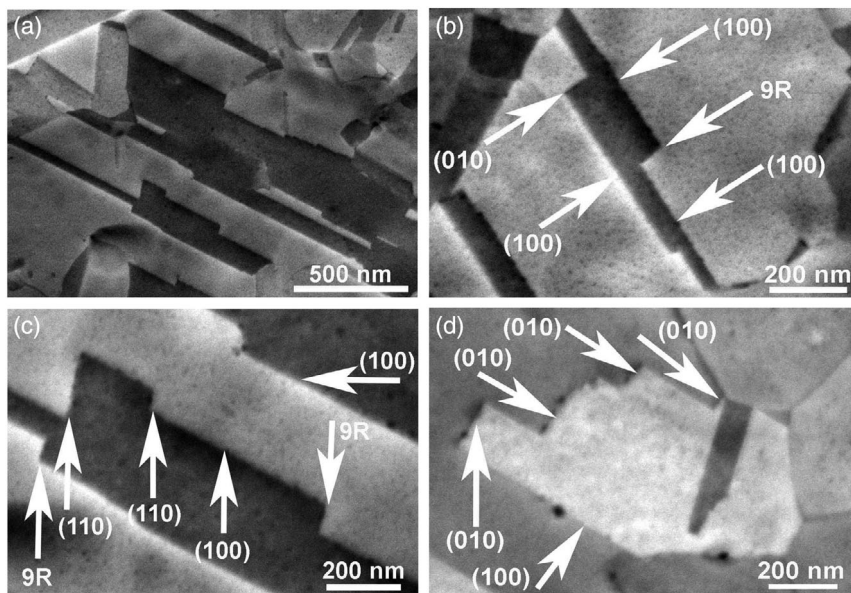
Figure 1. Continued.

Figure 2. SEM micrographs of twinned area deep in the HPT sample. Intersections of $(100)_{CSL}$ with other facets. a) Overall view. b) $(100)_{CSL}$, 9R and $(010)_{CSL}$ facets. c) $(100)_{CSL}$, 9R and $(110)_{CSL}$ facets. d) $(100)_{CSL}$ and $(010)_{CSL}$ facets.

are formation/decomposition of a solid solution,[50] transformations between intermetallic compounds,[51,52] amorphization or nanocrystallization,[53,54] etc. Usually, one can find the phases formed after SPD in the equilibrium phase diagrams at certain (mostly elevated) temperature T_{eff}.[47] We have to underline here that SPD is a highly nonequilibrium process and the steady state established during SPD is also highly nonequilibrium. Nevertheless, the equilibrium phase diagram is the only known

**ADVANCED
SCIENCE NEWS**

www.advancedsciencenews.com

**ADVANCED
ENGINEERING
MATERIALS**

www.aem-journal.com

instrument in our hands permitting to serve as a measure of this nonequilibrium. Particularly, T_{eff} is usually much higher than the temperature of SPD process T_{SPD} (T_{SPD} is frequently equal to the ambient one). The higher is the difference between T_{eff} and T_{SPD}, the larger is the deviation from equilibrium during SPD. This method to characterize the nonequilibrium steady state has been first proposed by Martin for the phase transformations driven by the severe neutron irradiation.[48] He proposed to find the phases appearing after irradiation (using their structure and composition) in the equilibrium phase diagrams and estimate the T_{eff} in such a way. In particular, in case of amorphization, the external treatment would be equal to the melting of a specimen.

We effectively used this approach to describe various transformations in the bulk phases.[2,50–57] However, the phase transitions can take place also in GBs. The examples are GB faceting–roughening,[62–64] wetting–dewetting,[108–110] prewetting,[63–67] premelting,[11,112] and pseudoincomplete wetting. This is a broad field for the investigations of SPD-driven phase

transitions. We can expect that, similar to the bulk phase diagrams, we will now be able to determine T_{eff} for the GB phase transitions. It would be interesting to know, for example, whether the T_{eff} values coincide for the bulk and GB phase transitions in the same alloy. However, to use the Martins approach, we need to know the GB phase diagrams in equilibrium, for example, without SPD treatment. Differently to the conventional bulk phase diagrams, the information about equilibrium GB phase diagrams is still quite scarce.[62–67,108–112] Therefore, we decided to start with the faceting–roughening transitions. In particular, they are the physical reason for the so-called transitions between special and general GBs.[113] Fortunately, the equilibrium phase diagram for the faceting–roughening transitions for the Σ3 twin GBs in copper is known.[64]

In **Figure 3**, two phase diagrams for the Σ3 GBs in 5N5 copper are shown. These are (T, θ) in Figure 3a and (T, φ) in Figure 3b interfacial stability diagrams for Σ3 {110} tilt GBs in copper plotted according to the approach by previous
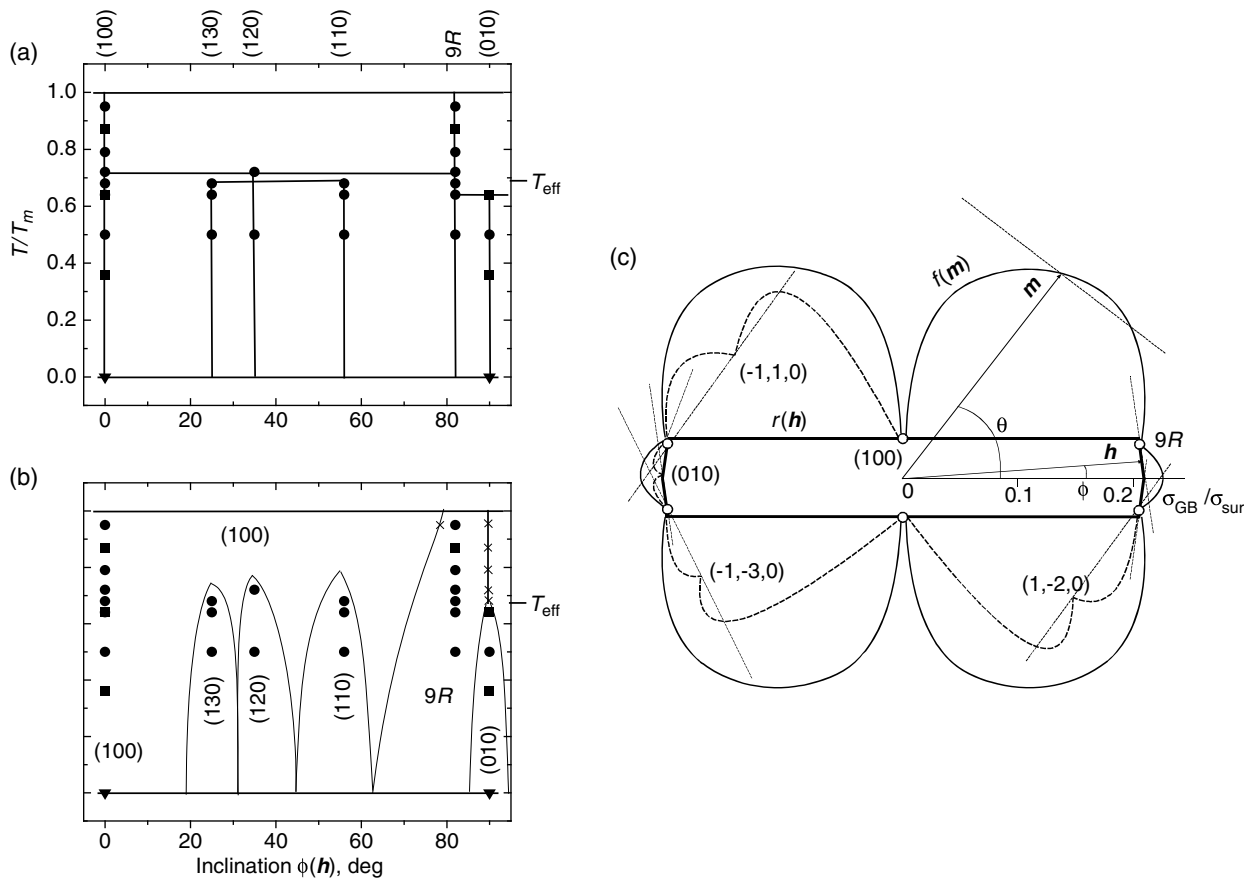

Figure 3. a) (T, θ) and b) (T, φ) interfacial stability diagrams for Σ3 {110} tilt GBs in Cu plotted according to the approach in a previous study.[64] θ and φ are angular variables, which measure interfacial orientation (m) and crystal shape (h), respectively, in an equatorial section perpendicular to the {110} tilt axis of the 3D stability diagram (see also c)).[64] The (T, θ) stability diagram (a) shows positions of cusps in the Wulff plot for $T < T_{Rf}$. The (T, φ) stability diagram b) plots the angular regions for the faceted areas of GB shape. Circles (●) and crosses (x) are the experimental data obtained from the study by Straumal et al.[64] ■ is the experimental data from previous studies,[114–122] ▼ is results of modeling.[117] c) Wulff–Herring energy diagram f(m) (thin solid line) and resulting equilibrium crystal shape r(h) (thick solid line) in plane section perpendicular to the {110} tilt axis for the Σ3 GBs in Cu at 1293 K.[64] Open circles represent the GB energy σ_{GB} for the (100)$_{CSL}$ and 9R facets measured with the aid of atomic force microscopy in the study by Straumal et al.[64] θ and φ are angular variables, which measure the interfacial orientation (m) and crystal shape (h), respectively. The cusps (dashed thin curves) for the (010)$_{CSL}$, (110)$_{CSL}$, (120)$_{CSL}$, and (130)$_{CSL}$ facets with perpendicular planes touching the r(h) are also shown. Reproduced with permission.[64] Copyright 2006, Elsevier

ADVANCED
SCIENCE NEWS

www.advancedsciencenews.com

ADVANCED
ENGINEERING
MATERIALS

www.aem-journal.com

study.[64] θ and ϕ are angular variables, which measure interfacial orientation and crystal shape, respectively, in an equatorial section perpendicular to the {110} tilt axis of the 3D stability diagram. The (T, θ) stability diagram (Figure 3a) shows positions of cusps in the Wulff plot for $T < T_R$. The (T, ϕ) stability diagram (Figure 3b) plots the angular regions for the faceted areas of GB shape. The shape of the "domes" in Figure 3b is rather similar to that of the existence areas for the special GBs in the coordinates "temperature"–"misorientation angle."[95] Circles • and crosses × are experimental data obtained in the study by Straumal et al.[64] ■ is the experimental data from previous studies.[114–122] ▼ are results of modeling.[123] Figure 3c shows Wulff–Herring energy diagram $f(m)$ (thin solid line) and resulting equilibrium crystal shape $r(h)$ (thick solid line) in plane section perpendicular to the {110} tilt axis for the Σ3 GBs in Cu at 1293 K.[64] It makes the sense of diagrams optically demonstrative as in Figure 3a,b.

Let us try to estimate the effective temperature T_{eff} for HPT of 5N5 copper by comparing our results shown in Figure 2 with phase diagrams shown in Figure 3. At the temperatures above 0.75 T_m, the Σ3 GBs in pure copper contain only two crystallographically different facets, namely $(100)_{CSL}$ and 9 R (Figure 3). In the present work, other types of facets are also observed. Thus, T_{eff} should be below 0.75 T_m. Figure 3 shows that four other facets $(110)_{CSL}$, $(120)_{CSL}$, $(130)_{CSL}$, and $(010)_{CSL}$ appear consecutively in the rather narrow temperature interval between 0.72 T_m and 0.63 T_m as the temperature decreases. In the present work, we observe only two of them, namely $(110)_{CSL}$, and $(010)_{CSL}$ and do not observe $(120)_{CSL}$ and $(130)_{CSL}$ ones. It means that T_{eff} is above 0.63 T_m. In such a way, we can estimate T_{eff} as lying between 0.72 and 0.63 T_m. Thus, $T_{eff} = 0.68 \pm 0.04\, T_m$ or $T_{eff} = 920 \pm 50$ K. This is the effective temperature for the pure copper undergoing HPT, obtained for the first time without "probe atoms."

Let us compare the value of T_{eff} obtained from GB faceting with the T_{eff} values obtained from the HPT-driven bulk phase transformations. The best candidate for this purpose is the competition between dissolution and precipitation of second-phase particles in the diluted copper-based solutions. The T_{eff} values measured with help of such transformations and, therefore, the "probe atoms" are analyzed in the study by Straumal et al.[50] In this work, the T_{eff} values are compared for various binary Cu-based alloys Cu–X. They were measured in investigations of competition between HPT-driven decomposition of solid solution and dissolution of precipitates. In the dynamic equilibrium, the rates of both processes become equal, and a certain steady-state concentration c_{ss} is established in the matrix. Then the c_{ss} value can be found in the equilibrium phase diagram Cu–X at the solvus line at a certain temperature T_{eff}. In other words, the c_{ss} is the concentration which establishes in a Cu–X solid solution after annealing at T_{eff}. In the study by Straumal et al.,[50] it has been shown that the T_{eff} values increase with increasing activation enthalpy for bulk diffusion of component X or with melting temperature T_m of component X. The lowest T_{eff} around 800 K was observed for copper alloyed with indium and tin. The highest T_{eff} of about 1300 K was observed for chromium and hafnium. Silver atoms are most close in their dimensions and properties to copper ones among components X studied in the study by

Straumal et al.[50] Indeed, T_{eff} for dissolution/precipitation of silver in copper is about 900 K.[57]

This value obtained for the HPT-driven bulk phase transition (namely the competition between dissolution and precipitation of second-phase particles) is very close for $T_{eff} = 920 \pm 50$ K obtained here for the GB faceting–roughening phase transition in the undoped copper. It means that the (nonequilibrium) structure of GBs formed during SPD-driven dynamic recrystallization in a steady state at T_{SPD} corresponds to the equilibrium GB structure at the elevated temperature T_{eff}. Moreover, T_{eff} for the bulk phase transformation is very close to that for the GB phase transformation. It means that the nature of various processes leading to the nonequilibrium structure of a material is the same in a SPD steady state.

4. Conclusion

The faceting–roughening GB transitions of coincident lattice GBs lead to the formation of different GB facets. Usually, these facets are parallel to the closely packed planes of CSLs. Different facets disappear at different roughening temperatures T_R. After HPT of high-purity 5N5 copper, the faceted Σ3 twins are formed containing four kinds of crystallographically different facets. The comparison of this fact with the known equilibrium stability diagram for the same 5N5 copper allowed us to estimate for the first time the effective temperature for pure copper during HPT processing being $T_{eff} = 920 \pm 50$ K. In other words, the HPT at RT forms Σ3 GB facets as if the sample has been annealed at $T_{eff} = 920 \pm 50$ K.

5. Experimental Section

For the investigations, the high purity (99.9995 wt% or 5N5) copper was used. The copper disks of 10 mm in diameter and 0.7 mm in thickness were subjected to the HPT at RT and 5 GPa for five rotations at 1 rpm in a Bridgman anvil-type unit with a quasiconstrained die using a custom-built computer controlled HPT device (W. Klement GmbH, Lang, Austria). After HPT, the thickness of the disks decreased from 0.7 to ≈0.4 mm and the diameter expanded from 10 to ≈12 mm. The microstructure characterization was conducted on the cross-sectional area of the disks. The samples for the investigations of microstructure were cut from the HPT-processed disks at a distance of 3 mm from the sample center. Conventional grinding using SiC paper down to 4000 grit and final mechanical polishing using 50 nm Al_2O_3 suspensions were conducted. Final electropolishing was conducted at RT in 14 M phosphoric acid by applying electric potential of 1.2 V. Time of about 2 min was sufficient to remove the damaged surface layer and reveal the grains. After electropolishing, the samples were rinsed with distilled water. The microstructure was characterized using high-resolution scanning electron microscopy (HRSEM, Zeiss Ultra Plus).

Conflict of Interest

The authors declare no conflict of interest.

Keywords

copper, faceting, grain boundaries, high pressure torsion, twins

[1] B. B. Straumal, A. R. Kilmametov, Y. Ivanisenko, A. A. Mazilkin, O. A. Kogtenkova, L. Kurmanaeva, A. Korneva, P. Zięba, B. Baretzky, *Int. J. Mater. Res.* **2015**, *106*, 657.

[2] K. Edalati, Z. Horita, *Acta Mater.* **2011**, *59*, 6831.

[3] B. B. Straumal, A. A. Mazilkin, S. G. Protasova, D. V. Gunderov, G. A. López, B. Baretzky, *Mater. Lett.* **2015**, *161*, 735.

[4] K. Bryła, J. Morgiel, M. Faryna, K. Edalati, Z. Horita, *Mater. Lett.* **2018**, *212*, 323.

[5] K. Edalati, D. J. Lee, T. Nagaoka, M. Arita, H. S. Kim, Z. Horita, R. Pippan, *Mater. Trans.* **2016**, *57*, 533.

[6] K. Edalati, Z. Horita, T. Furuta, S. Kuramoto, *Mater. Sci. Eng. A* **2013**, *559*, 506.

[7] K. Edalati, Y. Hashiguchi, P. H. R. Pereirac, Z. Horita, T. G. Langdon, *Mater. Sci. Eng. A* **2018**, *714*, 167.

[8] P. Krala, J. Dvorak, V. Sklenicka, T. Masuda, Z. Horita, K. Kucharova, M. Kvapilova, M. Svobodova, *Mater. Sci. Eng. A* **2018**, *723*, 287.

[9] S. Sabbaghianrad, S. A. Torbati-Sarraf, T. G. Langdon, *Mater. Sci. Eng. A* **2018**, *712*, 373.

[10] K. Tirsatine, H. Azzeddine, Y. Huang, T. Baudin, A.-L. Helbert, F. Brisset, D. Bradai, T. G. Langdon, *J. Alloys Compd.* **2018**, *753*, 46.

[11] M. Y. Alawadhi, S. Sabbaghianrad, Y. Huanga, T. G. Langdon, *J. Mater. Res. Technol.* **2017**, *6*, 369.

[12] M. Azabou, T. Makhlouf, J. Saurin, L. Escoda, J. J. Suñol, M. Khitouni, *Int. J. Adv. Manuf. Technol.* **2016**, *87*, 981.

[13] A. A. Mazilkin, B. B. Straumal, E. Rabkin, B. Baretzky, S. Enders, S. G. Protasova, O. A. Kogtenkova, R. Z. Valiev, *Acta Mater.* **2006**, *54*, 3933.

[14] B. Straumal, A. R. Kilmametov, Y. O. Kucheev, L. Kurmanaeva, Y. Ivanisenko, B. Baretzky, A. Korneva, P. Zięba, D. A. Molodov, *Mater. Lett.* **2014**, *118*, 111.

[15] Y. Huang, S. Sabbaghianrad, A. I. Almazrouee, K. J. Al-Fadhalah, S. N. Alhajeri, T. G. Langdon, *Mater. Sci. Eng. A* **2016**, *656*, 55.

[16] N. Lugo, N. Llorca, J. M. Cabrera, Z. Horita, *Mater. Sci. Eng. A* **2008**, *477*, 366.

[17] J. Čížek, M. Janeček, O. Srba, R. Kužel, Z. Barnovská, I. Procházka, S. Dobatkin, *Acta Mater.* **2011**, *59*, 2322.

[18] X. Z. Liao, Y. H. Zhao, Y. T. Zhu, R. Z. Valiev, D. V. Gunderov, *J. Appl. Phys.* **2004**, *96*, 636.

[19] M. Shamsborhan, M. Ebrahimi, *J. Alloys Compd.* **2016**, *682*, 552.

[20] C. L. Tang, H. Li, S. Y. Li, *Trans. Nonferrous Met. Soc. China* **2016**, *26*, 1736.

[21] Z. N. Mao, R. C. Gu, F. Liu, Y. Liu, X. Z. Liao, J. T. Wang, *Mater. Sci. Eng. A* **2016**, *674*, 186.

[22] E. Bagherpour, F. Qods, R. Ebrahimi, H. Miyamoto, *Mater. Sci. Eng. A* **2016**, *674*, 221.

[23] E. Bagherpour, F. Qods, R. Ebrahimi, H. Miyamoto, *Mater. Sci. Eng. A* **2016**, *666*, 324.

[24] P. C. Yadav, A. Sinhal, S. Sahu, A. Roy, S. Shekhar, *J. Mater. Eng. Perform.* **2016**, *25*, 2604.

[25] C. Xu, Z. Horita, T. G. Langdon, *Mater. Sci. Eng. A* **2011**, *528*, 6059.

[26] K. Edalati, D. Akama, A. Nishio, S. Lee, Y. Yonenaga, J. M. Cubero-Sesin, Z. Horita, *Acta Mater.* **2014**, *69*, 68.

[27] R. Tejedora, K. Edalati, J. A. Benito, Z. Horita, J. M. Cabrera, *Mater. Sci. Eng. A* **2019**, *743*, 597.

[28] I. F. Mohamed, T. Masuda, S. Lee, K. Edalati, Z. Horita, S. Hirosawa, K. Matsuda, D. Terada, M. Z. Omar, *Mater. Sci. Eng. A* **2017**, *704*, 112.

[29] K. Edalati, H. Shao, H. Emami, H. Iwaoka, E. Akiba, Z. Horita, *Int. J. Hydrogen Energy* **2016**, *41*, 8917.

[30] M. Isika, M. Niinomi, K. Cho, M. Nakai, H. Liu, H. Yilmazer, Z. Horita, S. Sato, T. Narushima, *J. Mech. Behav. Biomed. Mater.* **2016**, *59*, 226.

[31] M. Isik, M. Niinomi, H. Liu, K. Cho, M. Nakai, Z. Horita, S. Sato, T. Narushima, H. Yilmazer, M. Nagasako, *Mater. Trans.* **2016**, *57*, 1109.

[32] T. Hongo, K. Edalati, H. Iwaoka, M. Arita, J. Matsuda, E. Akiba, Z. Horita, *Mater. Sci. Eng. A* **2014**, *618*, 1.

[33] K. Edalati, K. Imamura, T. Kiss, Z. Horita, *Mater. Trans.* **2012**, *53*, 123.

[34] A. Hanna, H. Azzeddine, R. Lachha, T. Baudin, A.-L. Helbert, F. Brisset, Y. Huang, D. Bradai, T. G. Langdon, *J. Alloys Compd.* **2019**, *778*, 61.

[35] Y. I. Bourezg, H. Azzeddine, T. Baudin, A.-L. Helbert, Y. Huang, D. Bradai, T. G. Langdon, *Mater. Sci. Eng. A* **2018**, *724*, 477.

[36] P. Bazarnik, Y. Huang, M. Lewandowska, T. G. Langdon, *Mater. Sci. Eng. A* **2018**, *712*, 513.

[37] D. M. M. Cardona, J. Wongsa-Ngam, H. Jimenez, T. G. Langdon, *J. Mater. Res. Technol.* **2017**, *6*, 355.

[38] S. A. Torbati-Sarraf, S. Sabbaghianrad, R. B. Figueiredo, T. G. Langdon, *J. Alloys Compd.* **2017**, *712*, 185.

[39] M. Diez, H.-E. Kim, V. Serebryany, S. Dobatkin, Y. Estrin, *Mater. Sci. Eng. A* **2014**, *612*, 287.

[40] E. A. Lukyanova, N. S. Martynenko, I. Shakhova, A. N. Belyakov, L. L. Rokhlin, S. V. Dobatkin, Y. Z. Estrin, *Mater. Lett.* **2016**, *170*, 5.

[41] N. S. Martynenko, E. A. Luk'yanova, M. M. Morozov, V. S. Yusupov, S. V. Dobatkin, Y. Z. Estrin, *Metal Sci. Heat Treat.* **2018**, *60*, 253.

[42] T. Ungar, E. Schafler, P. Hanak, S. Bernstorff, M. Zehetbauer, *Mater. Sci. Eng. A* **2007**, *462*, 398.

[43] T. Ungár, E. Schafler, P. Hanák, S. Bernstorff, M. Zehetbauer, *Z. Metallkd.* **2005**, *96*, 578.

[44] R. O. Simmons, R. W. Balluffi, *Phys. Rev.* **1958**, *119*, 600.

[45] R. O. Simmons, R. W. Balluffi, *Phys. Rev.* **1960**, *117*, 52.

[46] R. O. Simmons, R. W. Balluffi, *Phys. Rev.* **1962**, *125*, 862.

[47] B. B. Straumal, A. A. Mazilkin, B. Baretzky, E. Rabkin, R. Z. Valiev, *Mater. Trans.* **2012**, *53*, 63.

[48] G. Martin, *Phys. Rev. B* **1984**, *30*, 1424.

[49] Y. Ashkenazy, N. Pant, J. Zhou, P. Bellon, R. S. Averback, *Acta Mater.* **2017**, *139*, 205.

[50] B. B. Straumal, A. R. Kilmametov, A. Korneva, A. A. Mazilkin, P. B. Straumal, P. Zięba, B. Baretzky, *J. Alloys Compd.* **2017**, *707*, 20.

[51] B. B. Straumal, A. R. Kilmametov, Y. O. Kucheev, K. I. Kolesnikova, A. Korneva, P. Zięba, B. Baretzky, *JETP Lett.* **2014**, *100*, 376.

[52] A. Korneva, B. Straumal, R. Chulist, A. Kilmametov, P. Bała, G. Cios, N. Schell, P. Zięba, *Mater. Lett.* **2016**, *179*, 12.

[53] A. A. Mazilkin, G. E. Abrosimova, S. G. Protasova, B. B. Straumal, G. Schütz, S. V. Dobatkin, A. S. Bakai, *J. Mater. Sci.* **2011**, *46*, 4336.

[54] B. B. Straumal, A. R. Kilmametov, A. A. Mazilkin, S. G. Protasova, K. I. Kolesnikova, P. B. Straumal, B. Baretzky, *Mater. Lett.* **2015**, *145*, 63.

[55] B. B. Straumal, A. R. Kilmametov, Y. O. Kucheev, L. Kurmanaeva, Y. Ivanisenko, B. Baretzky, A. Korneva, P. Zięba, D. A. Molodov, *Mater. Lett.* **2014**, *118*, 111.

[56] B. B. Straumal, S. G. Protasova, A. A. Mazilkin, E. Rabkin, D. Goll, G. Schütz, B. Baretzky, R. Valiev, *J. Mater. Sci.* **2012**, *47*, 360.

[57] B. B. Straumal, V. Pontikis, A. R. Kilmametov, A. A. Mazilkin, S. V. Dobatkin, B. Baretzky, *Acta Mater.* **2017**, *122*, 60.

**ADVANCED
SCIENCE NEWS**

www.advancedsciencenews.com

**ADVANCED
ENGINEERING
MATERIALS**

www.aem-journal.com

[58] D. A. Molodov, B. B. Straumal, L. S. Shvindlerman, *Scr. Metall.* **1984**, *18*, 207.

[59] B. B. Straumal, L. M. Klinger, L. S. Shvindlerman, *Scr. Metall.* **1983**, *17*, 275.

[60] Y. Ivanisenko, X. Sauvage, A. Mazilkin, A. Kilmametov, J. A. Beach, B. B. Straumal, *Adv. Eng. Mater.* **2018**, *20*, 1800443.

[61] A. A. Mazilkin, B. B. Straumal, A. R. Kilmametov, T. Boll, B. Baretzky, O. A. Kogtenkova, A. Korneva, P. Zięba, *Scr. Mater.* **2019**, *173*, 46.

[62] B. B. Straumal, O. A. Kogtenkova, A. S. Gornakova, V. G. Sursaeva, B. Baretzky, *J. Mater. Sci.* **2016**, *51*, 382.

[63] B. B. Straumal, S. A. Polyakov, E. Bischoff, W. Gust, E. J. Mittemeijer, *Interface Sci.* **2001**, *9*, 287.

[64] B. B. Straumal, S. A. Polyakov, E. J. Mittemeijer, *Acta Mater.* **2006**, *54*, 167.

[65] L.-S. Chang, B. B. Straumal, E. Rabkin, W. Gust, F. Sommer, *J. Phase Equilib.* **1997**, *18*, 128.

[66] L.-S. Chang, E. Rabkin, B. Straumal, P. Lejcek, S. Hofmann, W. Gust, *Scr. Mater.* **1997**, *37*, 729.

[67] L.-S. Chang, E. Rabkin, B. Straumal, S. Hoffmann, B. Baretzky, W. Gust, *Defect Diffus. Forum* **1998**, *156*, 135.

[68] J. Schölhammer, B. Baretzky, W. Gust, E. Mittemeijer, B. Straumal, *Interface Sci.* **2001**, *9*, 43.

[69] A. Kosinova, B. B. Straumal, A. R. Kilmametov, E. Rabkin, *Mater. Lett.* **2017**, *199*, 156.

[70] Y. Qi, A. Kosinova, A. R. Kilmametov, B. B. Straumal, E. Rabkin, *Mater. Charact.* **2018**, *145*, 1.

[71] H. Grimmer, W. Bollmann, D. T. Warrington, *Acta Cryst. A* **1974**, *30*, 197.

[72] B. B. Straumal, L. S. Shvindlerman, *Acta Metall.* **1985**, *33*, 1735.

[73] C. Minkwitz, C. Herzig, E. Rabkin, W. Gust, *Acta Mater.* **1999**, *47*, 1231.

[74] G. Wulff, *Z. Kristallogr.* **1901**, *34*, 449.

[75] C. Herring, in *Structure and Properties of Solid Surfaces* (Eds: R. Gomer, C. S. Smith), University of Chicago Press, Chicago **1952**, p. 5.

[76] L. D. Landau, E. M. Lifshitz, *Statistical Physics*, Vol. V, Addison-Wesley, Reading, MA **1958**.

[77] A. N. Aleshin, S. I. Prokofiev, L. S. Shvindlerman, *Scr. Metall.* **1985**, *19*, 1135.

[78] T. E. Hsieh, R. W. Balluffi, *Acta Metall.* **1989**, *37*, 2133.

[79] M. J. Kim, Y. K. Cho, D. Y. Yoon, *J. Am. Ceram. Soc.* **2004**, *87*, 455.

[80] C. Rottman, M. Wortis, *Phys. Rev. B* **1981**, *24*, 6274.

[81] C. Rottman, M. Wortis, *Phys. Rev. B* **1984**, *29*, 328.

[82] B. B. Straumal, V. N. Semenov, O. A. Kogtenkova, T. Watanabe, *Phys. Rev. Lett.* **2004**, *192*, 196101.

[83] K. O. Keshishev, A. Y. Parshin, A. V. Babkin, *Sov. Phys. JETP* **1981**, *53*, 362.

[84] U. Wolf, F. Ernst, T. Muschik, M. W. Finnis, H. F. Fischmeister, *Philos. Mag. A* **1992**, *66*, 991.

[85] F. Ernst, M. W. Finnis, D. Hoffmann, T. Muschik, U. Schönberger, U. Wolf, *Phys. Rev. Lett.* **1992**, *69*, 620.

[86] D. Hofmann, M. W. Finnis, *Acta Metall. Mater.* **1994**, *42*, 3555.

[87] A. Barg, E. Rabkin, W. Gust, *Acta Metall. Mater.* **1995**, *43*, 4067.

[88] B. B. Straumal, A. A. Mazilkin, B. Baretzky, E. Rabkin, R. Z. Valiev, *Mater. Trans.* **2012**, *53*, 63.

[89] A. A. Mazilkin, B. B. Straumal, E. Rabkin, B. Baretzky, S. Enders, S. G. Protasova, O. A. Kogtenkova, R. Z. Valiev, *Acta Mater.* **2006**, *54*, 3933.

[90] B. Straumal, A. R. Kilmametov, Y. O. Kucheev, L. Kurmanaeva, Y. Ivanisenko, B. Baretzky, A. Korneva, P. Zięba, D. A. Molodov, *Mater. Lett.* **2014**, *118*, 111.

[91] Y. Huang, S. Sabbaghianrad, A. I. Almazrouee, K. J. Al-Fadhalah, S. N. Alhajeri, T. G. Langdon, *Mater. Sci. Eng. A* **2016**, *656*, 55.

[92] N. Lugo, N. Llorca, J. M. Cabrera, Z. Horita, *Mater. Sci. Eng. A* **2008**, *477*, 366.

[93] J. Čížek, M. Janeček, O. Srba, R. Kužel, Z. Barnovská, I. Procházka, S. Dobatkin, *Acta Mater.* **2011**, *59*, 2322.

[94] X. Z. Liao, Y. H. Zhao, Y. T. Zhu, R. Z. Valiev, D. V. Gunderov, *J. Appl. Phys.* **2004**, *96*, 636.

[95] P. Zhao, B. Chen, J. Kelleher, G. Yuan, B. Guan, X. Zhang, S. Tu, *Acta Mater.* **2019**, *174*, 29.

[96] H. L. Yang, D. D. Wang, X. J. Zhu, Q. B. Fan, *Mater. Sci. Eng. A* **2019**, *759*, 203.

[97] Z. G. Zheng, X. Y. Zhang, L. Xie, L. G. Huang, T. Sun, *Metals* **2019**, *9*, 175.

[98] G. S. Zhang, Z. M. Zhang, X. B. Li, Z. M. Yan, X. Che, J. M. Yu, Y. Z. Meng, *J. Alloys Compd.* **2019**, *790*, 48.

[99] A. Ghorbani, A. Zarei-Hanzaki, P. D. Nezhadfar, M. H. Maghsoudi, *Int. J. Adv. Manuf. Technol.* **2019**, *102*, 5.

[100] X. X. Rao, Y. P. Wu, X. B. Pei, Y. H. Jing, L. Luo, Y. Liu, J. Lu, *Mater. Sci. Eng. A* **2019**, *754*, 112.

[101] L. W. Lu, X. Y. Liu, D. F. Shi, M. Ma, Z. C. Wang, *JOM* **2019**, *71*, 1566.

[102] Z. S. Wang, Y. J. Guan, T. Wang, Q. Zhang, X. T. Wei, X. Y. Fang, G. M. Zhu, S. Gao, *Mater. Sci. Eng. A* **2019**, *745*, 450.

[103] X. H. Zeng, P. Xue, L. H. Wu, D. R. Ni, B. L. Xiao, K. S. Wang, Z. Y. Ma, *J. Mater. Sci. Technol.* **2019**, *35*, 972.

[104] M. Suresh, A. Sharma, A. M. More, R. Kalsar, A. Bisht, N. Nayan, S. Suwas, *J. Alloys Compd.* **2019**, *785*, 972.

[105] F. Harati, M. Shamanian, M. Atapour, S. Hasani, J. A. Szpunar, *Mater. Res. Express* **2019**, *6*, 046559.

[106] A. P. Flausino Cibely, M. E. Landim Nassif, F. de Castro Bubani, P. H. R. Pereira, M. T. Paulino Aguilar, P. R. Cetlin, *Mater. Sci. Eng. A* **2019**, *756*, 474.

[107] X. Zhou, T. F. Ma, Y. L. Li, L. Li, K. X. Wang, Y. S. Zhang, Y. J. Lai, P. X. Zhang, *Mater. Sci. Eng. A* **2019**, *761*, 138046.

[108] E. I. Rabkin, L. S. Shvindlerman, B. B. Straumal, *Int. J. Mod. Phys. B* **1991**, *5*, 2989.

[109] B. Straumal, W. Gust, D. Molodov, *Interface Sci.* **1995**, *3*, 127.

[110] B. B. Straumal, W. Gust, T. Watanabe, *Mater. Sci. Forum* **1999**, *294/296*, 411.

[111] O. I. Noskovich, E. I. Rabkin, V. N. Semenov, B. B. Straumal, L. S. Shvindlerman, *Acta Metall. Mater.* **1991**, *39*, 3091.

[112] B. B. Straumal, O. I. Noskovich, V. N. Semenov, L. S. Shvindlerman, W. Gust, B. Predel, *Acta Metall. Mater.* **1992**, *40*, 795.

[113] E. L. Maksimova, L. S. Shvindlerman, B. B. Straumal, *Acta Metall.* **1988**, *36*, 1573.

[114] T. Y. Tan, S. L. Sass, R. W. Balluffi, *Philos. Mag.* **1975**, *31*, 575.

[115] F Ernst, M. W. Finnis, D. Hoffmann, T. Muschik, U. Schönberger, U. Wolf, *Phys. Rev. Lett.* **1992**, *69*, 620.

[116] D. S. Fisher, J. D. Weeks, *Phys. Rev. Lett.* **1983**, *50*, 1077.

[117] T. Muschik, W. Laub, M. W. Finnis, W. Gust, *Z. Metallkd.* **1993**, *84*, 596.

[118] T. Muschik, W. Laub, U. Wolf, M. W. Finnis, W. Gust, *Acta Metall. Mater.* **1993**, *41*, 2163.

[119] W. Laub, A. Oswald, T. Muschik, W. Gust, R. A. Fournelle, in *Solid–Solid Phase Transformations* (Ed: W. C. Johnson), The Minerals, Metals & Materials Society, Warrendale PA **1994**, p. 1115.

[120] A. Oswald, W. Laub, W. Gust, R. A. Fournelle, in *Solid–Solid Phase Transformations* (Ed: W.C. Johnson), The Minerals, Metals & Materials Society, Warrendale, PA **1994**, p. 1121.

[121] F. Ernst, M. W. Finnis, A. Koch, C. Schmidt, B. Straumal, W. Gust, *Z. Metallkd.* **1996**, *87*, 911.

[122] C. T. Forwood, L. M. Clarebrough, *Acta Metall.* **1984**, *32*, 757.

[123] L. M. Clarebrough, C. T. Forwood, *Phys. Status Solidi A* **1980**, *60*, 51.

1900589 (8 of 8)